

Surfactant-Stripped Micelles with Aggregation-Induced Enhanced Emission for Bimodal Gut Imaging In Vivo and Microbiota Tagging Ex Vivo

Zhen Jiang, Boyang Sun, Yueqi Wang, Heqi Gao, He Ren, Hao Zhang, Tong Lu, Xiangkui Ren, Wei Wei, Xiaoli Wang, Lei Zhang, Jiao Li, Dan Ding, Jonathan F. Lovell, and Yumiao Zhang*

Aggregation-induced emission luminogens (AIEgens) hold promise for biomedical imaging and new approaches facilitating their aggregation state are desirable for fluorescence enhancement. Herein, a series of surfactant-stripped AIEgen micelles (SSAMs) with improved fluorescence are developed by a low-temperature surfactant-stripping method to encapsulate AIEgens in temperature-sensitive Pluronic block copolymer. After stripping excessive surfactant, SSAMs exhibit altered optical properties and significantly higher fluorescence quantum yield. Using this method, a library of highly concentrated fluorescent nanoparticles are generated with tunable absorption and emission wavelengths, permitting imaging of deep tissues at different wavelengths. SSAMs remain physiologically stable and can pass safely through gastrointestinal tract (GI) without degradation in the harsh conditions, allowing for fluorescence and photoacoustic imaging of intestine with high resolution. D-amino acids (DAA), a natural metabolite for bacteria, can be chemically conjugated on the surface of SSAMs, enabling non-invasive monitoring of the microbial behavior of ex vivo fluorescently labeled gut microbiota in the GI tract.

applications such as biological probes,^[4–6] chemical sensing,^[7–9] organelle imaging,^[10] cancer cell labeling,^[11–13] photodynamic therapy,^[12] sterilization^[14] owing to the merits of fluorescence imaging such as high resolution, high selectivity and facile equipment. Encapsulated in nanoparticle form, AIEgens can avoid the fluorescence quenching phenomenon encountered with typical fluorogenic dyes, which is of great significance because for several applications fluorescent nanoparticles would be preferred over small fluorescent molecules. Many forms of nanoparticles have been developed for the encapsulation of AIEgens including liposome,^[15,16] polymeric nanoparticles,^[12,17–19] micelles,^[20,21] inorganic nanoparticles^[22] and others.^[23,24] Deliberate approaches to process AIEgen nanoparticles to further strengthen the aggregation state of AIEgens would be significantly useful for the development of brighter fluorogenic agents, but have been

rarely investigated, to the best of our knowledge. Furthermore, for gut imaging, where contrast agents in nanoparticle forms are likely to outperform small molecules, but AIEgens have rarely been used probably because small constituent molecules are

1. Introduction

Since the advent of some AIEgen use for biomedical imaging,^[1–3] AIEgens have emerged as a promising tool for a wide variety of

Z. Jiang, Y. Wang, H. Ren, H. Zhang, Prof. X. Ren, Prof. L. Zhang, Prof. Y. Zhang
School of Chemical Engineering and Technology
Key Laboratory of Systems Bioengineering
Ministry of Education
Tianjin University
Tianjin 300350, P. R. China
E-mail: ymzhang88@tju.edu.cn

B. Sun, Prof. J. F. Lovell
Department of Biomedical Engineering
The State University of New York at Buffalo
Buffalo, NY 14260, USA

H. Gao, Prof. J. Li, Prof. D. Ding
State Key Laboratory of Medicinal Chemical Biology
Key Laboratory of Bioactive Materials Ministry of Education and College of Life Sciences
Nankai University
Tianjin 300071, P. R. China

T. Lu
School of Precision Instrument and Opto-electronics Engineering
Tianjin University
Tianjin 300072, P. R. China

Prof. W. Wei
South China Normal University
Guangzhou, Guangdong Province 510631, P. R. China

Prof. X. Wang
Institute of Biomedical Engineering
Chinese Academy of Medical Sciences and Peking Union Medical College
Tianjin 300192, R. P. China

 The ORCID identification number(s) for the author(s) of this article can be found under <https://doi.org/10.1002/adhm.202100356>

DOI: 10.1002/adhm.202100356

prone to be metabolically absorbed in the intestine and few suitable oral delivery carriers are accessible.

Multimodal imaging of the GI tract is challenging,^[25] because the intestine, with its snaking nature deeply buried in the stomach, requires that imaging agents should be of high concentration enough and provide strong contrast for gut imaging.^[26,27] For deep tissue imaging, many probes in the second NIR window have been designed including downconversion nanoparticles,^[28] quantum dots,^[29,30] single wall nanotubes,^[31] semiconducting polymers,^[32] organic dye,^[33,34] bioconjugate^[35] since they can provide deeper penetration depth and higher resolution due to less photon scattering and autofluorescence.^[36] But as an ideal intestinal contrast agent, these probes should remain physiologically stable in the harsh GI conditions such as low pH in the stomach and degradative enzyme-rich environment in the intestine. For example, succinylated soy protein polymeric microcarrier integrating lanthanide-based downconversion nanoparticle has been reported for orally delivery of protein drugs and this type of carrier was shown to exhibit minimal leakage in the stomach and duodenum and prolonged residence time in the gut.^[37] In addition, a good contrast agent for gut imaging should not induce any significant side effects. Magnetic resonance imaging (MRI), and computed tomography (CT) are still the gold standard for the diagnosis of GI diseases in spite of some limitations such as high cost or exposure to ionizing radiation.^[38,39] Fluorescence imaging has the merits of low cost, easy of use, high resolution, high sensitivity, nonionizing radiation.^[40] Also, the FDA-approved dyes including indocyanine green and methylene blue have also demonstrated their potential for image-guided surgery practice. However, fluorescence imaging was limited by fluorescence quenching and penetration depth. Photoacoustic imaging is emerging as new imaging tool for molecular contrast imaging with deep penetration (over 10 cm) and good spatial resolution.^[41–46] Multimodal imaging modalities have been commonly used complementarily for functional imaging of intestine.^[28] Due to the complexity of the intestinal tract, 3D gut imaging and deep tissue imaging using AIE dots with high stability and brightness can provide a clearer understanding of the complex system of the gut.^[47]

Gut microbiota have been found to play a central role in many physiological and pathological activities.^[48,49] Microbiota transplants have shown promise for the treatment of clostridium difficile infection and intestinal diseases such as inflammatory bowel disease and irritable bowel syndrome.^[50,51] However, owing to lack of a good method to track the transplanted bacteria, investigation of their colonization and function with imaging and other approaches has been challenging. Fluorescence in situ hybridization (FISH) is used to label bacterial rRNA but this method involves fixation of cells.^[52] Gene expression of fluorescent protein is another approach for gut microbiota imaging but numerous gut bacteria are not readily amenable to genetic engineering.^[53] Metabolic labeling with alkyne-functional fluorophore conjugated with azido-sugars and azido-DAA via click chemistry has also been explored recently.^[54–56]

In the present work, we develop SSAMs by encapsulating a series of AIEgens in temperature-sensitive Pluronic micelles. At low temperature, free and loosely bound Pluronic, but not hydrophobic AIEgens themselves, undergo dissociation to unimers

and can be subsequently removed by centrifugal filtration.^[26] As we show here, after such surfactant-stripping processing, based on critical micelle concentration (CMC)-switching, SSAMs can be concentrated to a calculated optical absorbance close to 1000, evading the problem of penetration depth limitation, owing to extreme contrast for fluorescence and photoacoustic imaging of gut with high resolution. Importantly, the removal of excessive surfactant heightened the aggregation state of AIEgens, giving rise to significantly enhanced fluorescence. The surface of SSAM nanoparticles with many chemically active sites can be readily modified for the targeting properties. DAA, as a metabolic nutrient of many bacteria can be chemically conjugated to the surface of SSAMs by click chemistry, enabling fluorescent tagging of probiotics. SSAM-tagged *Lactococcus lactis* and *Lactobacillus* were orally administered in mice and their behaviors in GI tract were able to be investigated using the nanopatform of SSAMs. Thus, in this work we demonstrate that SSAMs shows promise for applications in gut microbiota imaging.

2. Results and Discussion

2.1. Preparation of Surfactant-Stripped AIEgen Micelles

Owing to temperature-sensitive micellization of Pluronic, when fluorophores are encapsulated in Pluronic F127 micelles, free micelles and loosely bound Pluronic can be removed, subject to low-temperature centrifugal filtration, leaving behind concentrated and purified SSAMs. As shown in Figure S1, Supporting Information, more than 99% of the free and loose Pluronic was effectively removed. Presumably, the hydrophobic fluorophores encapsulated in the SSAMs tend to be more aggregated after the removal of excess water-soluble Pluronic. Most fluorescent dyes are quenched when encapsulated in SSAMs due to the aggregation-caused quenching. However, AIEgens exhibited enhanced fluorescence when encapsulated in micelles. The surfactant-stripping process not only enables extremely concentrated AIEgens to be formed, but also results in significantly enhanced brightness (Figure 1a). The AIEgen hexaphenylsilole (HPS) was determined to work effective for SSAMs. As shown in Figure 1b, when normalized to the same concentration, HPS SSAMs were much more fluorescent after the surfactant-stripping processing, whereas HPS in DMSO was virtually non-fluorescent due to its good dispersion in the organic solvent, existing in non-aggregation state. The fluorescence enhancement by surfactant-stripping was also verified by the brighter color by naked eyes in the post-stripping samples as shown in Figure 1c. The absolute fluorescence quantum yield of HPS SSAMs can reach up to 82% after the majority of excess Pluronic F127 was effectively removed. We screened about twenty AIE dyes (refer to Table S1, Supporting Information for their chemical structures and names) and found that the fluorescence of five dyes was greatly enhanced by surfactant-stripping method based on emission intensity (Figure 1d). Others dyes were not hydrophobic enough to be encapsulated in F127 micelles or fluorescence was not enhanced by this method (Figure S2, Supporting Information). See Table S1, Supporting Information for the nomenclatures of AIEgens.

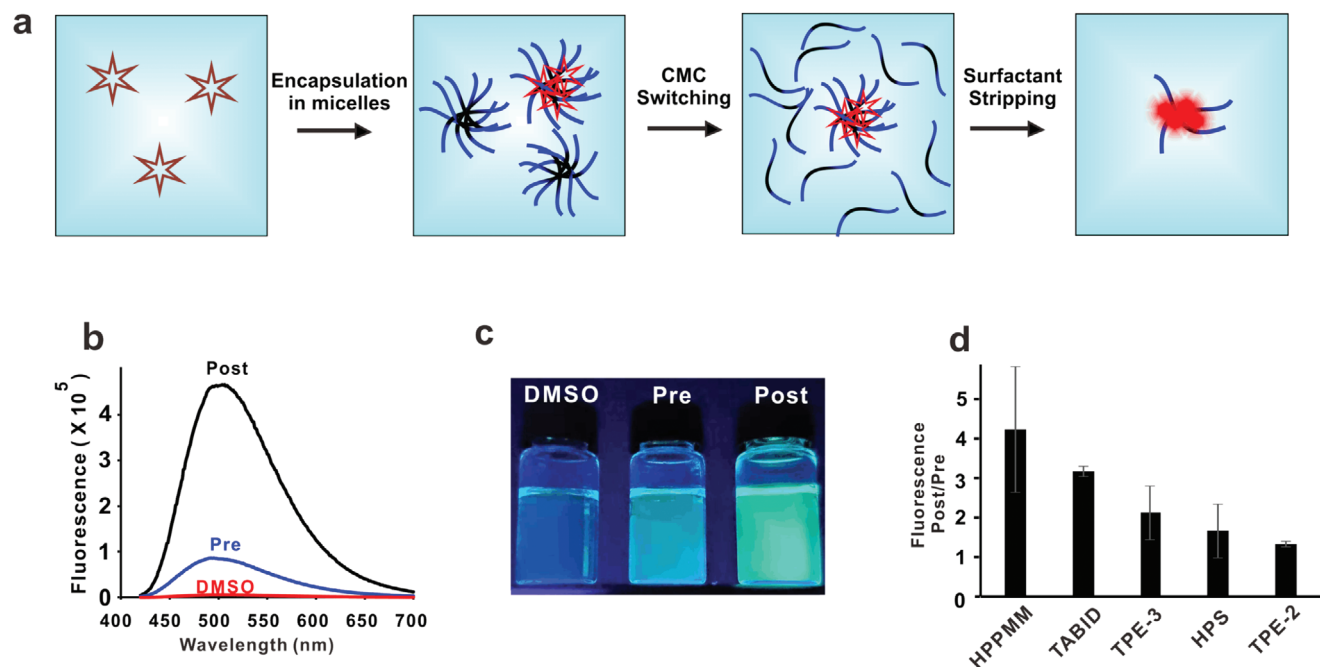


Figure 1. Generation of SSAMs with enhanced fluorescence. a) Schematic illustration of fluorescence enhancement by Pluronic micelles and surfactant-stripping at low temperature. Subject to CMC switching and removal of bulk surfactant, AIEgens were compacted more densely and increased brightness and concentration. b) Fluorescence spectrum of HPS in post-wash, pre-wash and in DMSO forms when normalized to the same mass. c) Photos of HPS in post-wash, pre-wash and in DMSO. d) After screening, 5 out of 20 AIEgens were identified that their fluorescence could be enhanced using surfactant-stripping approach by CMC-switching at low temperature. See Table S1, Supporting Information for the nomenclatures of AIEgens. Data are presented as mean±S.D. ($n = 3$).

2.2. Characterization of SSAMs

The removal of excess surfactant gave rise to altered fluorescence emission with red shift of 53 nm, which might be attributed to the rearrangement of the aggregated AIE dye in SSAMs (Figure 2a). We also measured the optical absorption of AIEgen dissolved in DMSO or formulated in Pluronic micelles or SSAMs. As shown in Figure 2b, HPS in the three types of formulations had maximum of absorption at 353, 360, 363 nm, respectively. Again, the blue shift after formulation and surfactant-stripping confirmed the altered rearrangement of HPS molecules inside micelles. Using this approach, we were able to obtain very concentrated AIEgen SSAMs with absorption close to 1000, while the pre-stripping sample can only reach to <10, as shown in Figure 2c. This is important because concentrated AIEgen SSAMs can provide sufficient contrast in a deeper body position without the limitation of penetration depth. Another advantage of this surfactant-stripping approach is that the absorption peak position did not display any significant change upon concentration of SSAMs, ensuring the accuracy of signal quantification (Figure 2d). This comparison was conducted by measuring concentrated SSAMs with a light path of 100 μm and diluted SSAMs (dilution factor is 100) with a light path of 1 cm. In contrast, conventional methods such as dissolving small molecules in solvent (e.g., water-soluble dyes in water) or excipients (e.g., gold nanorod in PEG) exhibited changed absorbance spectrum as previously reported.^[27] SSAMs formed from another AIEgen, (Z)-2-((4-(2-(4-methoxyphenyl)-1,2-diphenylvinyl)phenyl)(phenyl)methylene)malononitrile

(HPPMM), had a spherical morphology with diameter of around 40 nm revealed by electron microscopy (Figure 2e) and dynamic light scattering measurements (Figure 2f).

2.3. Generalization and Tunability

For biological applications, AIEgen SSAMs with longer absorption and fluorescent wavelengths are preferred, so we generalized this CMC-switching enhancement method to other hydrophobic AIEgens. By encapsulating different dyes such as HPPMM, TABID and AIE-787, AIE-786 (see Table S1, Supporting Information for full name and Figures S3–S4, Supporting Information for characterization including NMR and AIE other properties) in micelles, a family of AIEgen SSAMs were obtained with absorption maxima at 366, 413, 490, 610 and 740 nm (Figure 3a, top) and a digital photograph of these samples is shown at the bottom. Their emission wavelengths reached to 500, 607, 667, 930 and 1050 nm (Figure 3b), respectively. A normal photograph of these samples under UV lamps with excitation at 254 and 365 nm demonstrates their strong visible fluorescence, as shown in the bottom of the figure. Moreover, AIEgen SSAMs also have wide tunability by modifying chemical structures of AIEgens. For example, TABID dye and PABID dyes are structurally similar but TABID has two more methyl groups on aromatic rings (Table S1, Supporting Information). As shown in the Figure 3c, although PABID could form AIEgen SSAMs, the color was bleached and its fluorescence decreased after storage at 37 °C for 24 h. In contrast, TABID SSAMs exhibited better stability and the color and

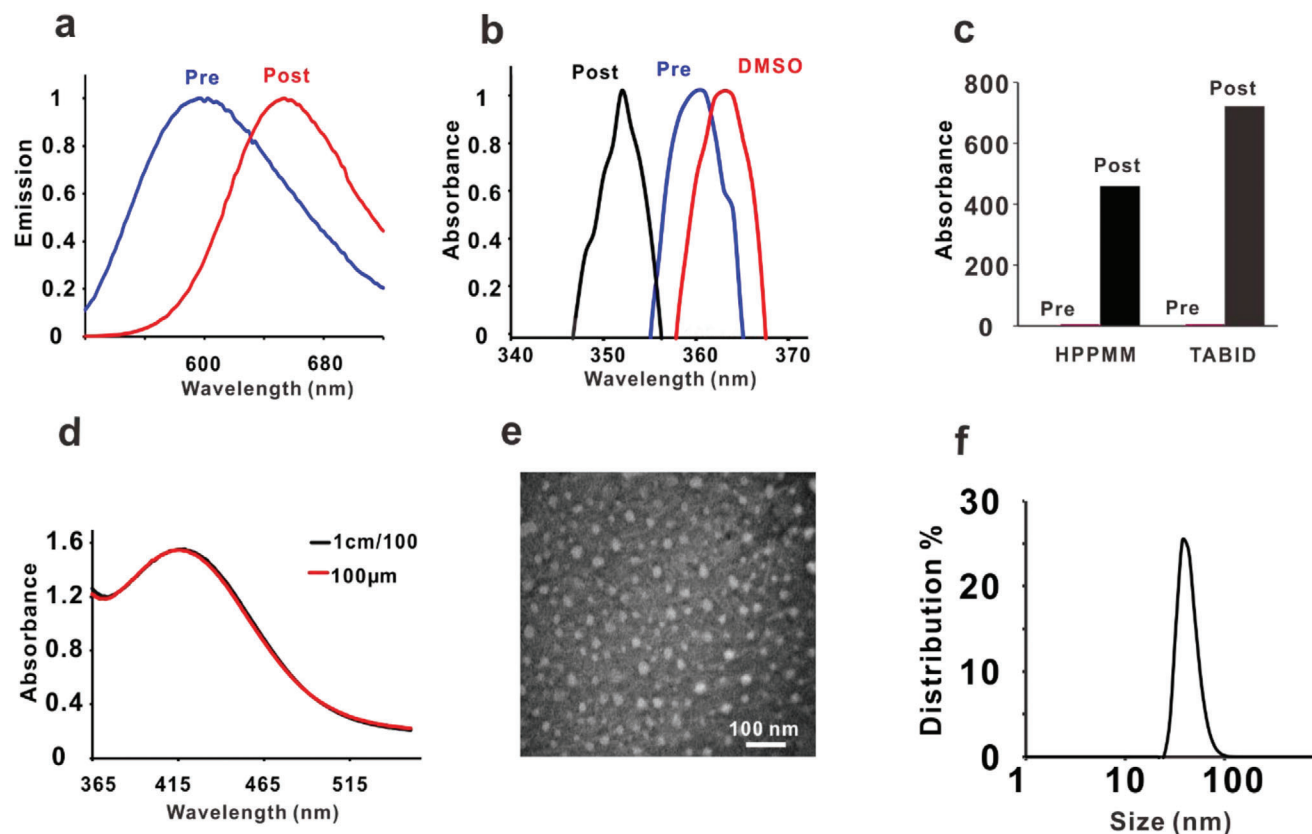


Figure 2. Characterization of AIEgen SSAMs. a) Fluorescence emission scan of TABID SSAMs before and after TABID micelles were subject to CMC-switching. Red shift occurred after CMC switching. b) Normalized absorption spectrum of HPS SSAMs before and after HPS micelles were subject to CMC-switching. Blue shift occurred for absorption spectrum after CMC-switching. c) TABID SSAM can be concentrated to absorption close to 800 and d) HPPMM SSAM without maxima wavelength shift during concentration process. e) TEM image and f) Dynamic light scattering measurement of HPPMM SSAMs. See Table S1, Supporting Information for the nomenclatures of AIEgens. Data are presented as mean \pm S.D. ($n = 3$).

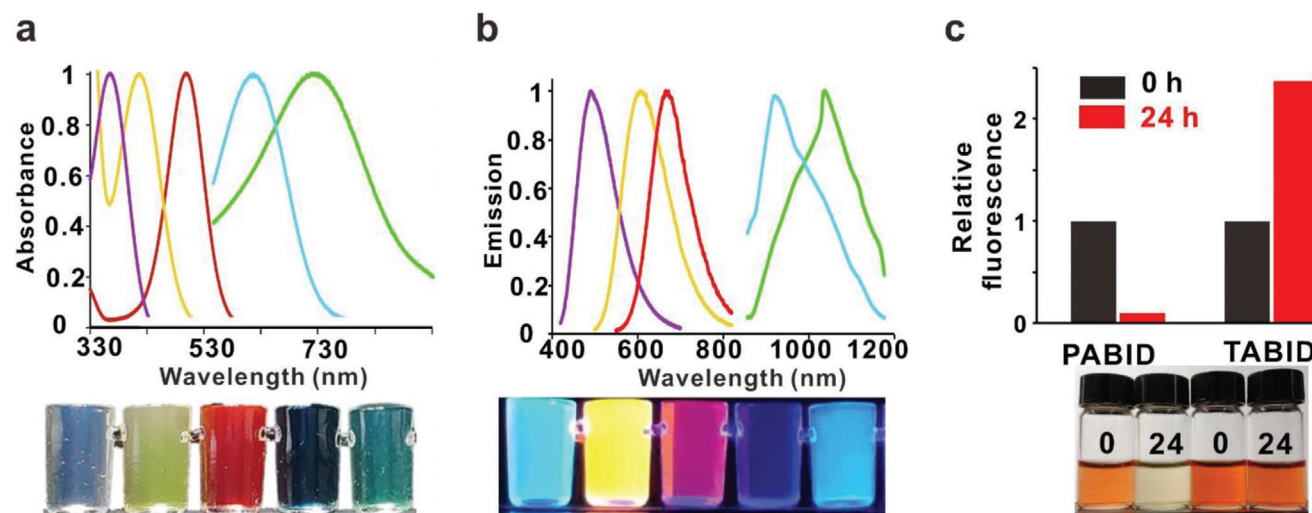


Figure 3. A family of SSAMs spanning the visible and near infrared spectrum. a) Normalized absorbance (top) and photograph (bottom) of different AIEgen SSAM aqueous solution. From left to right: HPS, HPPMM, TABID, AIE-787, and AIE-786. b) Normalized fluorescence (top) and photograph (bottom) of different AIEgen SSAM aqueous solution. From left to right: HPS, HPPMM, TABID, AIE-787 and AIE-786 with excitation by two UV lamps at 254 and 365 nm. c) Fluorescence of PABID SSAMs is not stable but TABID is. Relative fluorescence (top) and photos (bottom) of PABID SSAMs and TABID SSAMs 24 h after preparation compared with pre-CMC-switching.

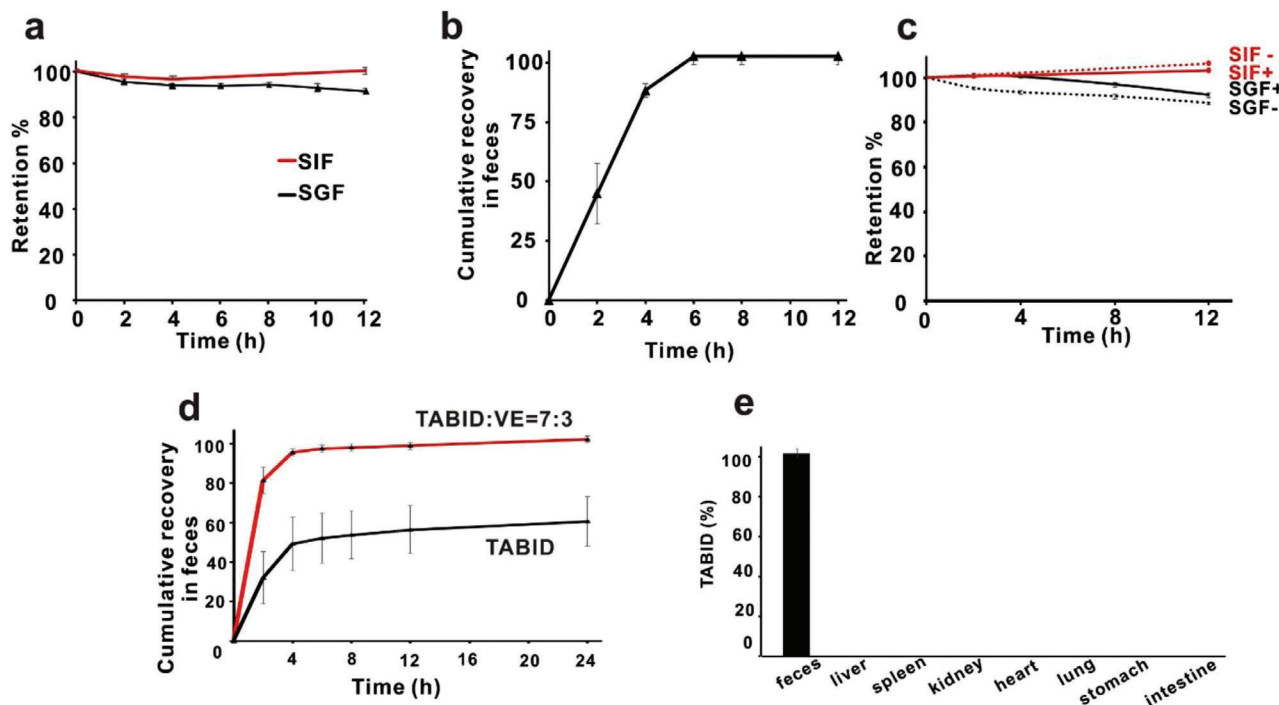


Figure 4. Gut stability of SSAMs in vitro and in vivo. a) Retention of HPPMM SSAMs in SGF (black) and SIF (red) at 37 °C. b) Recovery of HPPMM SSAMs in feces after oral administration in mice. When co-loaded with vitamin E, TABID SSAMs showed enhanced stability c) in vitro and d) in vivo. e) Biodistribution of TABID in main organs after mice were orally administered TABID SSAMs. It was demonstrated that micelles were almost 100% excreted by feces with undetectable amount in main organs. Data are presented as mean±S.D. ($n = 3$).

fluorescence remained unchanged. This could be explained by the fact that the introduction of methyl groups increased the hydrophobic interaction of dye and micelles, giving rise to enhanced stability.

2.4. Stability in GI Tract In Vitro and In Vivo

In order to assess the suitability of AIEgen SSAMs for use as contrast agents for intestinal imaging, the potential of withstanding the harsh environment in gastrointestinal tract was investigated in vitro and in vivo. As shown in Figure 4a, HPPMM SSAMs showed no absorbance decrease when incubated in simulated gastric fluid (SGF) and simulated intestinal fluid (SIF) for at least 12 h, indicating the stability of HPPMM SSAMs at low pH and in the degradative enzyme-enriched environment of the GI tract. This was also verified by an in vivo experiment in which all dyes were fully recovered from feces 12 h after mice were orally given 30 O.D. (about 1.3 mg) (optical density; defined as the amount of dye required to produce an absorption of 1 at the peak wavelength measured in a 1 cm path length) HPPMM SSAMs (Figure 4b). The good stability in the GI tract could be attributed to the polyethylene oxide (PEO) component of the F127 structure on the surface of micelles. For the TABID AIEgen, although its SSAMs were stable in SIF for 12 h as shown in Figure 4c, the stability in SGF measured by absorbance was <80% after 24-h incubation.

To improve the stability in acidic condition, we adopted a co-loading strategy that a more hydrophobic nutrition supple-

ment was co-encapsulated with TABID in SSAMs. After screening various supplements including coenzyme Q10 (Q10), vitamin A (VA), vitamin D (VD), and vitamin E (VE) (Figure S5, Supporting Information), the formulation of 30% (wt%) VE as co-loader was found to fully preserve TABID SSAMs stability in SGF for at least 12 h (Figure 3c) and could increase the TABID recovery in feces from 50% to 100% within 24 h after administering 100 O.D. (about 1.2 mg in 200 μ L) TABID SSAMs in mice (Figure 4d). The co-loader enhancement has been observed to a range of surfactant-stripped micelles,^[57,58] and is likely explained by additional molecular interaction between the co-loader and TABID within the micelles. The complete excretion of the contrast agent, with no dye was detectable in main organs including liver, spleen, kidney, heart and lungs, stomach, intestine (Figure 4e), which is consistent with our prior finding of orally-administered surfactant-stripped micelles^[27] and gut confinement presents advantages for imaging intestinal processes and contrast agent safety.

2.5. Fluorescence Imaging and Photoacoustic Imaging of Intestine

Encouraged by these results, we next investigated the capability of HPPMM SSAMs for use as contrast agent for intestinal imaging. First, we gavaged 30 O.D. (1.3 mg in 200 μ L) HPPMM SSAMs in mice in the experiment group or gave PBS to control group. Feces were collected and imaged under fluorescence microscope. As shown in Figure 5a (bottom), the feces from

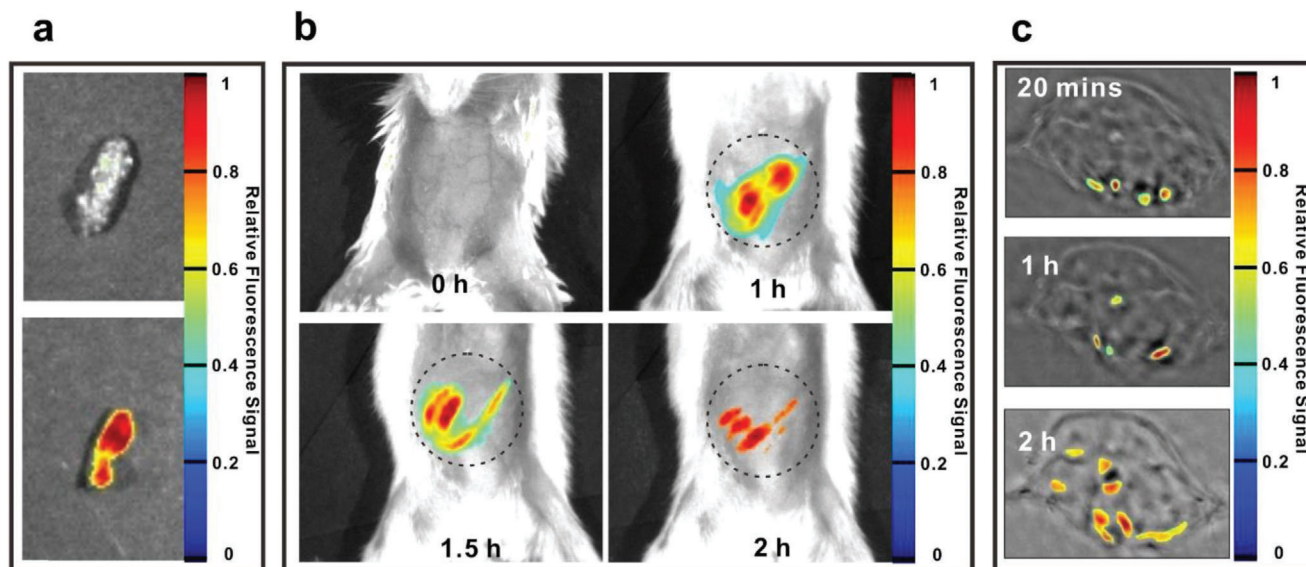


Figure 5. Fluorescence imaging and photoacoustic imaging of intestine a) Images of feces collected from mice given PBS (top) or HPPMM SSAMs (bottom). b) Fluorescence imaging of intestine at indicated time of points after mice were given HPPMM SSAMs. c) Photoacoustic imaging of intestine at indicated time of points after mice were given 30 O.D. (3.2 mg in 200 μ L) AIE-786 SSAMs.

the group given AIEgen SSAMs fluorescently glowed strongly, whereas those from the control group did not under the same imaging condition (Figure 5a, top). Then we imaged the gut of the mice orally administered 30 O.D. (1.3 mg in 200 μ L) HPPMM SSAMs. No fluorescence signal was observed in the pre-scan mice (Figure 5b) but after 1, 1.5, 2 h, the contour of the intestine could clearly be visualized, as well as the change in localization of the fluorescence intensity as the contrast agent transited along in GI tract. Although the fluorescence emission wavelength of HPPMM SSAMs is at the short end of the near infrared spectra at 700 nm, high signal-to-noise intestinal fluorescence imaging was facilitated by the high concentration of the contrast agent generated enabled by the CMC-switching method, which could overcome the limitation of penetration depth considering the snaking structure of the intestines. After testing the stability of AIE-786 SSAMs (absorbance peak of 740 nm) in vitro (Figure S6, Supporting Information), we also obtained the intestinal images at different time points using photoacoustic tomography method as shown in Figure 5c.

2.6. Ex Vivo Labeled Gut Microbiota

After demonstrating the utility of SSAMs for contrast imaging of the gut, we next used SSAMs as imaging tool to observe the gut microbiota in GI tract. As a necessary building block for peptidoglycans (PGN), DAA have been shown to be able to efficiently label bacteria in vitro and in vivo.^[54,59,60] Therefore, we first conjugated DAA on the surface of Pluronic micelles as illustrated in Figures S7 and S8, Supporting Information. We chose facultative anaerobic *Lactococcus lactis* and *Lactobacillus plantarum* as models of transplanted gut bacteria that are generally recognized as safe for orally administration and used for metabolic engineering (Figure 6a). One advantage of SSAM-labeled bacteria over small molecule labeled bacteria is the former could remain stable in

the gastrointestinal conditions. As shown in Figure 6b, we used FITC-labeled *Lactobacillus plantarum* as the control and found that its fluorescence significantly decreased to zero once mixed in SGF. After 24 h in SIF, luminescence decreased almost 40%. By contrast, The fluorescence intensity retention of TABID (co-loaded with VE) SSAMs labeled bacteria in SGF and SIF were much higher than the control group. It is likely because AIEgens are encapsulated in micelles and avoid direct exposure like small molecules to the harsh environment in GI. As shown in Figure 6c, DAA-conjugated SSAMs can be efficiently labeled in vitro on the surface of *Lactococcus lactis* and *Lactobacillus plantarum*, as revealed by confocal images. DAA is essential for metabolic activities of bacterial peptidoglycans and also well-tolerated by the PGN construction-related enzymes.^[55] After metabolic labeling by DAA, *Lactococcus lactis* remained alive evidenced by cell division. As shown in Figure S9, Supporting Information, the flow cytometry quantification of the mean fluorescence intensity of a single cell decreased over time as bacteria divided.^[60–62] With abundant SSAMs in culture medium, fluorescence decrease rate is slower compared to the scenario without SSAMs because new fluorogenic SSAMs were metabolically incorporated onto bacterial cell surfaces. Although the serial fluorescence dilution with bacterial division limits the timeframe of microbiome detection within several hours, we were able to image the transplanted gut bacteria in vivo (Figure 6d) and ex vivo (Figure 6e) 2 h after oral administration of *Lactococcus lactis*. Then main organs including heart, lung, kidney, liver, and spleen were collected. And no noticeable fluorescence was observed in main organs when subject to and fluorescently imaging, indicating that the DAA-SSAM has not been absorbed into body (Figure 6f). Then gut microbiota was recovered from small intestine, and then subjected to confocal imaging. As shown in Figure 6g, the contour of bacteria could be clearly seen in the DAPI or SSAM channels for confocal images suggesting that the fluorescence observed in Figure 6c,d was from DAA-SSAM labeled bacteria. Further investigation is

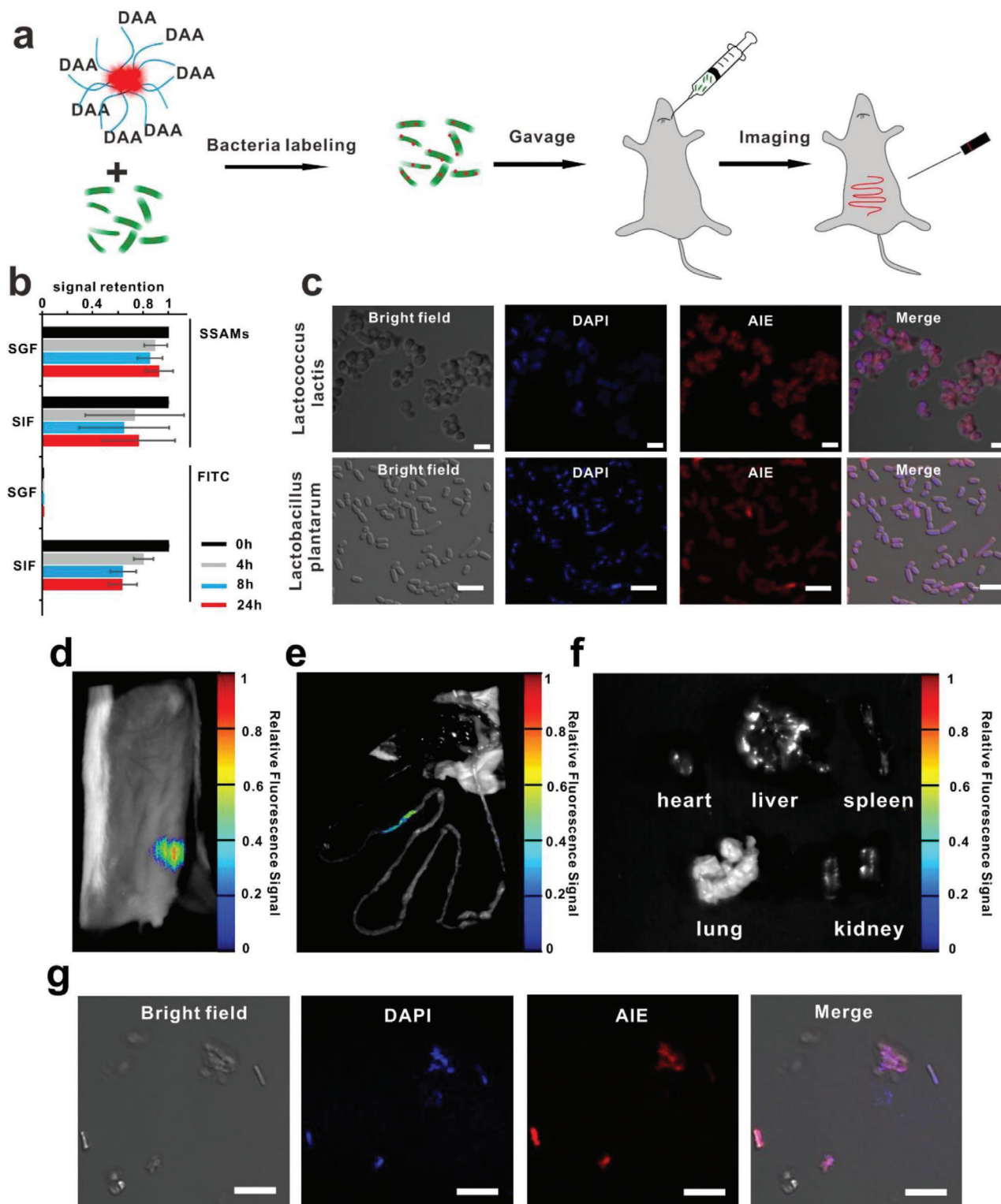


Figure 6. SSAMs for ex vivo gut microbiota tagging. a) Schematic illustration of preparing SSAMs for targeting of gut microbiota. b) Fluorescence retention of SSAMs labeled bacteria and FITC labeled bacteria in SGF and SIF. c) Confocal images of *Lactococcus lactis* and *Lactobacillus plantarum* incubated with TABID SSAMs. Scale bars, 5 μ m. DAPI and AIE channels were for bacterial nucleus staining and SSAMs. d) In vivo fluorescence imaging of labeled gut microbiota in intestine 2 h after mice were orally given SSAM-labeled *Lactococcus lactis*. Ex vivo fluorescence imaging of e) gut and f) main organs including heart, liver, spleen, lung, and kidney. g) Confocal images of labeled *Lactobacillus plantarum* recovered from small intestine 2 h after mice were orally given SSAM-labeled bacteria. DAPI and AIE channels were for bacterial nucleus staining and SSAMs. Scale bars, 5 μ m. Data are presented as mean \pm S.D. ($n = 3$).

planned to shed light on the rate of SSAMs shedding from bacteria and the survival percentage of the transplanted gut bacteria when imaging, but this work demonstrates proof-of-concept that SSAM is able to be used as a new imaging tool for the studies of specific gut bacteria in a host.

3. Conclusion

In this work, we developed a surfactant-stripped AIEgen micelle platform that both enhances the aggregation state and brightness of AIEgens after the removal of excessive surfactant, and enables AIEgen concentration to high levels. After AIEgen screening, five SSAMs were developed with tunable absorbance and emission wavelength spanning the visible to near infrared spectrum. They can remain photo-stable and physiologically stable in the biochemical environment of the gut. SSAMs were effective for bimodal imaging of the intestine. The surface of SSAMs could be conjugated with DAA used in microbial metabolism, thus enabling DAA-conjugated SSAMs to be used as an imaging tool to investigate the behavior of transplanted gut microbiota in GI tract. Compared to conventional nanoparticles or small molecules, SSAMs have many advantages in one single nanoparticle, which is of importance for the applications of in vivo gut imaging and ex vivo bacteria labeling: i) SSAMs could remain stable and protect fluorophores from rapid degradation like small molecules such as FITC in gastrointestinal conditions. ii) CMC-switching approach could greatly enhance fluorescence of conventional AIEgen-encapsulated Pluronic micelles due to the more aggregated state of AIEgens; iii) SSAMs represent a family of multicolor nanoparticles with similar chemical and physical properties. iv) SSAMs have exceptionally concentration in NIR for effective and background-free GI imaging. v) Various targeting moieties could be chemically modified with ease on the surface of SSAMs, proving useful tools for functional study of gut. Altogether the SSAM platform represents a new tool for molecular imaging of intestinal physiology and microbiota.

4. Experimental Section

Materials: Pluronic F127 (Sigma, America); Sodium phosphotungstate hydrate (Aladdin); 9,10-diphenylanthracene (J&K Scientific, Beijing, China); Pepsin (Yuanye, Shanghai, China); Trypsin (Yuanye, Shanghai, China); Coenzyme Q10 (Yuanye, Shanghai, China); P-nitrophenyl chloroformate, NPC(Alfa); 3-azido-1-propanamine (Energy, Shanghai, China); D-propargylglycine (Meryer, Shanghai, China); 1,3-indandione (Meryer, Shanghai, China); Triethylamine (Meryer Shanghai, China); Hexaphenylsilole, HPS, (Dingxian, Shanghai, China); 4-[N,N-di(p-tolyl)amino]benzaldehyde (Dingxian, Shanghai, China); Vitamin K1, VK1 (Aladdin); Vitamin A (Bide, Shanghai, China); β -carotene (Heowns, Tianjin, China); Sodium ascorbate (Heowns, Tianjin, China); 4-(N,N-Diphenylamino) benzaldehyde (Heowns, Tianjin, China); Ninhydrin (Heowns, Tianjin, China); Vitamin D (Feiyu, Nantong, China); Vitamin E (Macklin); Copper sulfate pentahydrate (Kemio, Tianjin, China); and DAPI (Solarbio, Beijing, China); FITC (Solarbio, Beijing, China)

Experimental Protocols—Synthesis of AIEgens: PABID was synthesized according to a previous report.^[63] The synthetic route of TABID was similar to PABID except using 4-[N,N-di(p-tolyl)amino]benzaldehyde as reactant instead of 4-(N,N-Diphenylamino) benzaldehyde. Briefly, An acetone-trile solution (15 mL) of 4-[N,N-di(p-tolyl)amino]benzaldehyde (200 mg) and 1,3-indandione (116 mg), triethylamine (355 mg) was stirred at 45 °C for 2 h. Collect the precipitate by suction filtration and wash them with cold

methanol (3 × 100 mL). The pure product was obtained as red powders in 27.6% yield (83 mg). NMR spectrum was collected on Bruker AVANCE IIIITM HD 400 MHz Nano Bay. TPE-1, TPE-2, TPE-3, AIE-4 were kindly provided by Xiangkui Ren's group at Tianjin University. HPPMM was kindly provided by Professor Xinggui Gu at Beijing University of Chemical Engineering. AIE-786 and AIE-787 were provided by Professor Dan Ding at Nankai University.

Preparation of SSAMs: AIEgens (1 mg) were dissolved in methylene chloride (DCM) and the resulting solution was added to 10 mL Pluronic F127 (10% wt/vol) and stirred for three hours. To remove free and loosely bound F127, CMC switching was conducted by ultracentrifugation. Briefly the pre-wash solution was pre-cooled in 4 °C freezer and then subjected to centrifugal ultrafiltration (molecular weight cutoff of 100 kDa) at 4 °C until around 200 μ L of solution was retained. Water was added back to the concentrate for the next round of washing. And the ultrafiltration procedure was repeated for three times. To improve the stability of TABID in SGF and SIF, co-loading strategy was employed, briefly, 1mg TABID with different mass ratios of VE (mass ratio of TABID:VE (mg: mg) = 10:0; 9:1; 8:2; 7:3) were dissolved in 1 mL DCM and added to 10 mL Pluronic F127 (10% wt/vol) aqueous solution by stirring for 3 h. And the centrifugal ultrafiltration process is the same as mentioned above.

Characterization of SSAMs: Size measurement was carried out with dynamic light scattering using a Nano ZS90 Zeta sizer (Malvern Instruments). Transmission electron microscopy was performed using a TEM-1400Flash Transmission electron microscope negatively stained with 1% sodium phosphotungstate hydrate. Absorbance was measured with spectrophotometer (Thermo Fisher Evolution 201 UV-vis) using cuvettes with 1 cm light path. For the measurement of concentrated SSAMs, non-standard cuvettes with 0.1 mm was used. The calculated absorbance was calculated by multiplying the factor of 100 (1 cm/0.1 mm). Fluorescence properties were assessed using an Infinite 200 Pro (Tecan group Ltd, Switzerland) spectrofluorometer. Absolute fluorescence quantum yield was collected using a Horiba FluoroMax Plus Spectrofluorometer equipped with a Quanta- ϕ integrating sphere accessory.

Stability of SSAMs In Vitro and In Vivo: To assess the stability of the SSAM in SGF and SIF, concentrated SSAMs were diluted into the simulated fluids and the final absorbance was close to 1, then dialyzed against 200 mL SGF with 3.2 g L⁻¹ pepsin added and 10 g L⁻¹ pancreatin-containing SIF at 37 °C for 24 h. Absorbance was measured at different time points for the determination of retention and stability of SSAMs 8-week-old CD-1 mice were purchased from Charles River Beijing Co., Ltd (Beijing, China). All animal experiments were performed in accordance with Tianjin University Institutional Animal Care and Use Committee (Protocol number: TJUE-2020-189).

For the determination of the stability of SSAMs in intestine in vivo, 6–8 weeks female CD1 mice ($n = 3$) were fasted overnight prior to use with access to water. After gavage of 30 O.D. (1.3 mg in 0.2 mL distilled water, figure 4B) of HPPMM SSAMs or 100 O.D. (1.2 mg in 0.2 mL distilled water, figure 4B) of TABID SSAMs, mice were transferred to metabolic cages, and feces were collected. For the determination of recovery, feces were dissolved in 4 mL of organic solvent (chloroform) in test tubes. Feces were homogenized using a homogenizer (Hangzhou Younging, YN-J01-038) until the AIEgen were dissolved completely. The solution was filtered through gauze until clear and the absorbance was measured for the determination of AIEgen mass in different tissues.

Fluorescence Imaging and Photoacoustic Imaging of Intestine: For fluorescence imaging of intestine and feces, 30 O.D. (1.3 mg in 200 μ L) of HPPMM SSAM was gavaged in CD-1 mice. Fluorescence images were acquired in with an automated in vivo imaging system (Maestro). Mice in the control group were given PBS as control.

For photoacoustic imaging of intestine, 30 O.D. (3.16 mg in 200 μ L) of AIE-786 SSAMs (maximum absorbance: 740 nm) were gavaged. Images were collected by a customized imaging system set up in Jiao Li's group.^[64] A multi-spectral photoacoustic imaging system was used. Briefly, a tunable optical parametric oscillator pumped by an Nd:YAG laser provides excitation pulses with a duration of 6 ns at wavelengths from 680 to 1064 nm. The wavelength of 700 nm is used with the pulse energy of 80 mJ. Four arms of a fiber bundle provide uniform illumination. For

ultrasound detection, a cylindrical focused ultrasound transducer with a center frequency of 3.5 MHz is used.

Chemical Modification of Surface of SSAMs: The synthesis route was shown in Figure S5, Supporting Information: For the synthesis of NPC-F127: 10 g F127 was put into vacuum at 120 °C overnight before use. Then the dye F127 was dissolved in 15 mL anhydrous benzene. 967 mg p-nitrophenyl chloroformate (NPC) was dissolved in another 15 mL anhydrous benzene. The NPC solution was added in F127 solution dropwise and the solution was stirred at room temperature under argon for 36 h. For purification, the solution was precipitated in 10-fold excessed cold ether for three times and NPC-F127 was obtained from precipitate.

For the synthesis of F127-N₃: 1g NPC-F127 and 30 mg 3-azido-1-propanamine dissolved in 10 mL anhydrous dichloromethane and stirred overnight at room temperature. Dichloromethane was removed by rotating evaporation, and then put into dialysis bag with 8000–14 000 Da molecular weight cutoff against water to remove unreacted small molecules. After dialysis for 24 h, the solution was freeze-dried overnight and stored in fridge for further use.

For the synthesis of F127-DAA: a mixture of 1 g F127-N₃, 18 mg D-propargylglycine (DPG), 12.5 mg copper sulfate pentahydrate, 49.5 mg sodium ascorbate, was dissolved in 10 mL water and 10 mL methanol. The mixture was stirred at room temperature overnight. The methanol was removed by rotary evaporation, the precipitation was removed by centrifugation, the clean supernatant was put into a dialysis bag with 8000–14 000 Da molecular weight cut-off against unreacted molecules for 24 h, then freeze-drying was conducted to obtain the powder of the product.

To demonstrate successful attachment of amino acids to F127 terminals, ninhydrin was used for the quantification of DAA. Specifically, a mixture of 5 mL pH = 6 phosphate buffer, 2 mL 2% ninhydrin ethanol solution, 2 mL sample, and 5 mL ethanol were added to a 25 mL colorimetric cylinder and heated at 100 °C for 15 min, and then immediately put into cool water for 10 min. Water was added back to keep the volume of the brown solution to be 25 mL. Absorbance at 568 nm was used for quantification. Calibration curve was shown as Figure S6, Supporting Information. For the preparation of DAA-conjugated SSAMs, F127-DAA instead of F127 was used and other procedure remained the same.

Bacteria Tagging and Ex Vivo Imaging: *Lactococcus lactis* (NZ9000) was kindly provided by Professor Jianjun Qiao's group at Tianjin university. *Lactobacillus* (ATCC 8014) was kindly provided by Professor Yunzi Luo's group at Tianjin university. *L. Lactis* (or *Lactobacillus*) were grown overnight in 7 mL M17 (or MRS) medium and reached the plateau stage. 2×10^7 CFUs/0.2 mL of bacterial solution were re-injected into 7 mL of M17 (or MRS) and then co-cultured with 0.2 mL (14 O.D.) DAA-conjugated TABID co-loaded SSAMs in the dark for 2 h. After that, the fluorescently labeled bacteria were collected by centrifugation at 500 rcf for 5 minutes and washed with 1 × PBS three times. After resuspension in 1 mL PBS, the bacteria were prepared for gavage or testing fluorescence retention in SGF and SIF. Finally, 6.5×10^5 CFUs in 0.2 mL SGF or SIF SSAMs labeled *Lactobacillus* was measured by fluorescence intensity at 0, 4, 8, 24 h. 1 mL of 0.01 mg mL^{-1} FITC in pH = 9 NaOH solution was used to resuspend 7.8×10^7 CFUs of *Lactobacillus* to label bacteria as a control. After incubation in shaker at 37 °C for 2 h under darkness, unreacted FITC was then washed by PBS for 3 times. Finally, the fluorescence retention of 9.5×10^6 CFUs FITC labeled bacteria in 0.2 mL SGF or SIF was measured at 0, 4, 8, 24 h. 6.5×10^8 CFUs/0.2 mL for *Lactococcus lactis* were orally administered in CD-1 mice. Fluorescence images were taken after gavage for 2 h on IVIS fluorescence imaging system (NIGHT OWL IILB983, Berthold Technologies) using 488 nm laser and 660 nm detector filter.

For the single-cell imaging of gavigated bacteria in gut (in Figure 6d,e), TABID co-loaded DAA-conjugated SSAMs were gavigated in mice, and 2 h later, mice were sacrificed and duodenum was excised. PBS was used to flush the sectioned intestine, stainless steel mesh with mesh number of 100 (Dongmai), 300 (Dongmai), 1800 (Lvruo) was used to filter the debris and feces for the collection of bacteria PBS solution. Afterwards, 50 mL of the bacteria was used for the preparation of confocal images.

Flow Cytometry and Confocal Imaging: After incubation with abundant DAA-conjugated TABID SSAMs for two hours, one of two group was left unchanged, and for the other group, the medium was replaced with blank

medium without DAA-conjugated TABID SSAMs. 1 mL of bacterial solution was sampled every 2 h and the medium was removed and resuspended in PBS for flow cytometry (FACSAria III) using 488nm laser and 695nm fluorescence detector.

For confocal imaging in vitro in Figure 6c, 1 mL labeled bacterial suspension was stained with DAPI for 10 min, then subject to centrifugation (500 g, 5 min) and wash for three times with 1 × PBS. For confocal imaging (Nikon A1R+), 488 nm excitation light was used and detector channel between 635 and 685 nm was selected.

Statistical Analysis: All the quantitative data were presented as mean ± SD. The mean values are based on at least three replicates. Normalization of data was carried out for Figure 2a, b, 3a, b, and 6b.

Supporting Information

Supporting Information is available from the Wiley Online Library or from the author.

Acknowledgements

The authors thank Professor Jianjun Qiao and Yunzi Luo for providing *Lactococcus Lactis* and *Lactobacillus plantarum*. The authors also thank Professor Xinggui Gu for gifting HPPMM, Prof. Jianlan Jiang for the comments on manuscript. This work was supported by the National Natural Science Foundation of China (32071384) and Tianjin Municipal Government of China (19JCQNJC12800).

Conflict of Interest

The authors declare no conflict of interest.

Author Contributions

Z.J., B.S., J.F.L., and Y.Z. conceived and designed the project. Z.J., Y.W., H.R., and H.Z. conducted most experiments. X.R., H.G., and D.D. designed and synthesized AIE dyes. T.L., J.L., W.W., and X.W. contributed to PA and fluorescence imaging and data analysis. Z.J., L.Z., J.F.L., and Y.Z. wrote the draft and all authors revised the manuscript and perform data analysis.

Data Availability Statement

Research data are not shared.

Keywords

AIEgens, gut imaging, gut microbiota, surfactant-stripped micelles

Received: February 25, 2021

Revised: June 14, 2021

Published online: June 23, 2021

- [1] J. Luo, Z. Xie, J. W. Y. Lam, L. Cheng, B. Z. Tang, H. Chen, C. Qiu, H. S. Kwok, X. Zhan, Y. Liu, D. Zhu, *Chem. Commun.* **2001**, 2001, 1740.
- [2] J. Mei, N. L. C. Leung, R. T. K. Kwok, J. W. Y. Lam, B. Z. Tang, *Chem. Rev.* **2015**, 115, 11718.
- [3] J. Mei, Y. Hong, J. W. Y. Lam, A. Qin, Y. Tang, B. Z. Tang, *Adv. Mater.* **2014**, 26, 5429.

- [4] W. Fu, C. Yan, Y. Zhang, Y. Ma, Z. Guo, W.-H. Zhu, *Front. Chem.* **2019**, *7*, 291.
- [5] W. Fu, C. Yan, Z. Guo, J. Zhang, H. Zhang, H. Tian, W.-H. Zhu, *J. Am. Chem. Soc.* **2019**, *141*, 3171.
- [6] M. Gao, H. Su, S. Li, Y. Lin, X. Ling, A. Qin, B. Z. Tang, *Chem. Commun.* **2017**, *53*, 921.
- [7] R. Li, L. Yan, Z. Wang, Z. Qi, *J. Mol. Struct.* **2017**, *1136*, 1.
- [8] J. Sun, J. Cao, J. Wang, J. Wang, S. Wang, *Sens. Actuators, B* **2019**, *293*, 159.
- [9] P. Guan, B. Yang, B. Liu, *Spectrochim. Acta, Part A* **2020**, *225*, 117604.
- [10] S. Li, X. Ling, Y. Lin, A. Qin, M. Gao, B. Z. Tang, *Chem. Sci.* **2018**, *9*, 5730.
- [11] J. Ni, P. Zhang, T. Jiang, Y. Chen, H. Su, D. Wang, Z. Yu, R. T. K. Kwok, Z. Zhao, J. W. Y. Lam, B. Z. Tang, *Adv. Mater.* **2018**, *30*, 1805220.
- [12] J. Dai, Y. Li, Z. Long, R. Jiang, Z. Zhuang, Z. Wang, Z. Zhao, X. Lou, F. Xia, B. Z. Tang, *ACS Nano* **2020**, *14*, 854.
- [13] J. Liu, C. Chen, S. Ji, Q. Liu, D. Ding, D. Zhao, B. Liu, *Chem. Sci.* **2017**, *8*, 2782.
- [14] D. Mao, F. Hu, S. J. Kenry, W. Wu, D. Ding, D. Kong, B. Liu, *Adv. Mater.* **2018**, *30*, 1706831.
- [15] Y. Yang, L. Wang, H. Cao, Q. Li, Y. Li, M. Han, H. Wang, J. Li, *Nano Lett.* **2019**, *19*, 1821.
- [16] X. Zhang, B. Wang, Y. Xia, S. Zhao, Z. Tian, P. Ning, Z. Wang, *ACS Appl. Mater. Interfaces* **2018**, *10*, 25146.
- [17] Y. Li, Z. Cai, S. Liu, H. Zhang, S. T. H. Wong, J. W. Y. Lam, R. T. K. Kwok, J. Qian, B. Z. Tang, *Nat. Commun.* **2020**, *11*, 1255.
- [18] Y. Li, D. Hu, Z. Sheng, T. Min, M. Zha, J.-S. Ni, H. Zheng, K. Li, *Biomaterials* **2021**, *264*, 120365.
- [19] X. Zhang, K. Wang, M. Liu, X. Zhang, L. Tao, Y. Chen, Y. Wei, *Nanoscale* **2015**, *7*, 11486.
- [20] W.-C. Wu, C.-Y. Chen, Y. Tian, S.-H. Jang, Y. Hong, Y. Liu, R. Hu, B. Z. Tang, Y.-T. Lee, C.-T. Chen, W.-C. Chen, A. K.-Y. Jen, *Adv. Funct. Mater.* **2010**, *20*, 1413.
- [21] C. Zhang, S. Jin, S. Li, X. Xue, J. Liu, Y. Huang, Y. Jiang, W.-Q. Chen, G. Zou, X.-J. Liang, *ACS Appl. Mater. Interfaces* **2014**, *6*, 5212.
- [22] Z. Wu, Q. Yao, O. J. H. Chai, N. Ding, W. Xu, S. Zang, J. Xie, *Angew. Chem.* **2020**, *132*, 10020.
- [23] N. Alifu, A. Zebibula, J. Qi, H. Zhang, C. Sun, X. Yu, D. Xue, J. W. Y. Lam, G. Li, J. Qian, B. Z. Tang, *ACS Nano* **2018**, *12*, 11282.
- [24] J. Qi, C. Sun, D. Li, H. Zhang, W. Yu, A. Zebibula, J. W. Y. Lam, W. Xi, L. Zhu, F. Cai, P. Wei, C. Zhu, R. T. K. Kwok, L. L. Streich, R. Prevedel, J. Qian, B. Z. Tang, *ACS Nano* **2018**, *12*, 7936.
- [25] X. Dang, N. M. Bardhan, J. Qi, L. Gu, N. A. Eze, C.-W. Lin, S. Kataria, P. T. Hammond, A. M. Belcher, *Sci. Rep.* **2019**, *9*, 3873.
- [26] Y. Zhang, D. Wang, S. Goel, B. Sun, U. Chitgupi, J. Geng, H. Sun, T. E. Barnhart, W. Cai, J. Xia, J. F. Lovell, *Adv. Mater.* **2016**, *28*, 8524.
- [27] Y. Zhang, M. Jeon, L. J. Rich, H. Hong, J. Geng, Y. Zhang, S. Shi, T. E. Barnhart, P. Alexandridis, J. D. Huizinga, M. Seshadri, W. Cai, C. Kim, J. F. Lovell, *Nat. Nanotech* **2014**, *9*, 631.
- [28] L. Ma, S. Huang, S. He, Z. Wang, Z. Cheng, *Biosens. Bioelectron.* **2020**, *151*, 112000.
- [29] A. Zebibula, N. Alifu, L. Xia, C. Sun, X. Yu, D. Xue, L. Liu, G. Li, J. Qian, *Adv. Funct. Mater.* **2018**, *28*, 1703451.
- [30] Y. Zhang, G. Hong, Y. Zhang, G. Chen, F. Li, H. Dai, Q. Wang, *ACS Nano* **2012**, *6*, 3695.
- [31] A. L. Antaris, J. T. Robinson, O. K. Yaghi, G. Hong, S. Diao, R. Luong, H. Dai, *ACS Nano* **2013**, *7*, 3644.
- [32] J. Wu, L. You, L. Lan, H. J. Lee, S. T. Chaudhry, R. Li, J.-X. Cheng, J. Mei, *Adv. Mater.* **2017**, *29*, 1703403.
- [33] A. L. Antaris, H. Chen, K. Cheng, Y. Sun, G. Hong, C. Qu, S. Diao, Z. Deng, X. Hu, B. Zhang, X. Zhang, O. K. Yaghi, Z. R. Alamparambil, X. Hong, Z. Cheng, H. Dai, *Nat. Mater.* **2016**, *15*, 235.
- [34] N. Bhutiani, A. Samyukty, K. M. McMasters, N. K. Egilmez, L. R. McNally, *Photoacoustics* **2019**, *13*, 46.
- [35] S. Zhu, S. Herraiz, J. Yue, M. Zhang, H. Wan, Q. Yang, Z. Ma, Y. Wang, J. He, A. L. Antaris, Y. Zhong, S. Diao, Y. Feng, Y. Zhou, K. Yu, G. Hong, Y. Liang, A. J. Hsueh, H. Dai, *Adv. Mater.* **2018**, *30*, 1705799.
- [36] L. Liu, S. Wang, B. Zhao, P. Pei, Y. Fan, X. Li, F. Zhang, *Angew. Chem., Int. Ed.* **2018**, *57*, 7518.
- [37] R. Wang, L. Zhou, W. Wang, X. Li, F. Zhang, *Nat. Commun.* **2017**, *8*, 14702.
- [38] C. E. Dye, R. R. Gaffney, T. M. Dykes, M. T. Moyer, *Am. J. Med.* **2012**, *125*, 1228.e1.
- [39] F.-Z. Cui, J.-H. Liu, Y. Liu, B.-Y. Yuan, X. Gong, Q.-H. Yuan, T.-T. Gong, L. Wang, *Chinese J. Anal. Chem.* **2020**, *48*, 1004.
- [40] R. Weissleder, V. Ntziachristos, *Nat. Med.* **2003**, *9*, 123.
- [41] Z. Wang, P. K. Upputuri, X. Zhen, R. Zhang, Y. Jiang, X. Ai, Z. Zhang, M. Hu, Z. Meng, Y. Lu, Y. Zheng, K. Pu, M. Pramanik, B. Xing, *Nano Res.* **2019**, *12*, 49.
- [42] Z. Wang, X. Zhen, P. K. Upputuri, Y. Jiang, J. Lau, M. Pramanik, K. Pu, B. Xing, *ACS Nano* **2019**, *13*, 5816.
- [43] Q. Miao, Y. Lyu, D. Ding, K. Pu, *Adv. Mater.* **2016**, *28*, 3662.
- [44] Q. Fu, R. Zhu, J. Song, H. Yang, X. Chen, *Adv. Mater.* **2018**, *31*, 1805875.
- [45] J. Lin, M. Wang, H. Hu, X. Yang, B. Wen, Z. Wang, O. Jacobson, J. Song, G. Zhang, G. Niu, P. Huang, X. Chen, *Adv. Mater.* **2016**, *28*, 3273.
- [46] Z. Yang, Y. Dai, C. Yin, Q. Fan, W. Zhang, J. Song, G. Yu, W. Tang, W. Fan, B. C. Yung, J. Li, X. Li, X. Li, Y. Tang, W. Huang, J. Song, X. Chen, *Adv. Mater.* **2018**, *30*, 1707509.
- [47] J. Qi, N. Alifu, A. Zebibula, P. Wei, J. W. Y. Lam, H.-Q. Peng, R. T. K. Kwok, J. Qian, B. Z. Tang, *Nano Today* **2020**, *34*, 100893.
- [48] E. C. Martens, M. Neumann, M. S. Desai, *Nat. Rev. Microbiol.* **2018**, *16*, 457.
- [49] S. Drouault, G. Corthier, S. D. Ehrlich, P. Renault, *Appl. Environ. Microbiol.* **1999**, *65*, 4881.
- [50] S. Paramsothy, M. A. Kamm, N. O. Kaakoush, A. J. Walsh, J. van den Bogaerde, D. Samuel, R. W. L. Leong, S. Connor, W. Ng, R. Paramsothy, W. Xuan, E. Lin, H. M. Mitchell, T. J. Borody, *Lancet* **2017**, *389*, 1218.
- [51] P. H. Johnsen, F. Hilpüsch, J. P. Cavanagh, I. S. Leikanger, C. Kolstad, P. C. Valle, R. Goll, *Lancet Gastroenterol. Hepatol.* **2018**, *3*, 17.
- [52] M. E. V. Johansson, G. C. Hansson, in *Mucins* (Eds: M. A. McGuckin, D. J. Thornton), Humana Press, Totowa, NJ, **2012**, pp. 229–235.
- [53] W. R. Whitaker, E. S. Shepherd, J. L. Sonnenburg, *Cell* **2017**, *169*, 538.
- [54] S. E. Pidgeon, J. M. Fura, W. Leon, M. Birabaharan, D. Vezenov, M. M. Pires, *Angew. Chem., Int. Ed.* **2015**, *54*, 6158.
- [55] E. Kuru, H. V. Hughes, P. J. Brown, E. Hall, S. Tekkam, F. Cava, M. A. de Pedro, Y. V. Brun, M. S. VanNieuwenhze, *Angew. Chem.* **2012**, *124*, 12687.
- [56] E. Kuru, C. Lambert, J. Rittichier, R. Till, A. Ducret, A. Derouaux, J. Gray, J. Biboy, W. Vollmer, M. VanNieuwenhze, Y. V. Brun, R. E. Sockett, *Nat. Microbiol.* **2017**, *2*, 1648.
- [57] U. Chitgupi, N. Nyayapathi, J. Kim, D. Wang, B. Sun, C. Li, K. Carter, W. Huang, C. Kim, J. Xia, J. F. Lovell, *Adv. Mater.* **2019**, *31*, 1902279.
- [58] B. Sun, U. Chitgupi, C. Li, J. Federizon, C. Zhang, D. M. Ruszaj, A. Razi, J. Ortega, S. Neelamegham, Y. Zhang, J. F. Lovell, *Adv. Therap.* **2020**, *3*, 1900161.
- [59] M. D. Lebar, J. M. May, A. J. Meeske, S. A. Leiman, T. J. Lupoli, H. Tsukamoto, R. Losick, D. Z. Rudner, S. Walker, D. Kahne, *J. Am. Chem. Soc.* **2014**, *136*, 10874.
- [60] W. Wang, L. Lin, Y. Du, Y. Song, X. Peng, X. Chen, C. J. Yang, *Nat. Commun.* **2019**, *10*, 1317.
- [61] G. J. Britton, J. J. Faith, *Nat. Med.* **2015**, *21*, 977.
- [62] I. Jarchum, *Nat. Methods* **2015**, *12*, 908.
- [63] S. Redon, G. Eucat, M. Ipy, E. Jeanneau, I. Gautier-Luneau, A. Ibanez, C. Andraud, Y. Bretonnière, *Dyes Pigm.* **2018**, *156*, 116.
- [64] T. Lu, T. Chen, F. Gao, B. Sun, V. Ntziachristos, J. Li, *J. Biophotonics* **2021**, *14*, e202000325.